Near-Inertial Energy Propagation from the Mixed Layer: Theoretical Considerations

VASSILIS ZERVAKIS AND MURRAY D. LEVINE

College of Oceanic and Atmospheric Sciences, Oregon State University, Corvallis, Oregon

(Manuscript received 5 April 1994, in final form 11 November 1994)

ABSTRACT

Wind-generated inertial currents can radiate from the mixed layer as horizontally and vertically propagating near-inertial internal gravity waves. To study the timescale of the decay of mixed layer energy and the magnitude of the energy transfer to the ocean below, the authors developed a numerical, linear model on a β plane, using baroclinic modes to describe the velocity field. The model is unforced—wave propagation is initiated by specifying the mixed layer currents that would be generated by a moving atmospheric front. The numerical results are interpreted using concepts of modal interference and modal departure that can be evaluated analytically, thereby permitting predictions of some features of wave field evolution without the need to run the numerical model. The energy exchange with the pycnocline and deep ocean is explored as a function of the propagation speed and direction of the front, the horizontal extent of the storm, and the background stratification.

The timescale of energy transfer from the mixed layer to the pycnocline due to modal interference is greatly affected by the β effect, causing much faster energy transfer for currents generated by southward propagating fronts. The timescale is typically not a strong function of mixed layer depth; however, the magnitude of the energy transfer is. Besides modal interference, vertical energy propagation occurs when low modes leave the area—a possibility for storms of finite horizontal extent. The deep stratification and f also affect the timescale; climatological examples indicate faster wave evolution at low latitudes.

1. Introduction

Near-inertial oscillations are a commonly observed feature in the world's oceans. Nearly circular motions in a horizontal plane with a frequency near f (the local Coriolis parameter) are often excited by the passage of atmospheric fronts. In the mixed layer, wind generation of near-inertial oscillations has been quite successfully explained by simple models based on treating the mixed layer as a solid slab (e.g., Pollard and Millard 1970; Kundu 1976; D'Asaro 1985; Paduan et al. 1989). However, the decay of near-inertial energy in the mixed layer is not understood as well as the generation. Possible mechanisms responsible for the decrease in mixed layer energy include radiation of linear internal gravity waves, nonlinear transfer of energy to other frequency bands, and local turbulent dissipation.

This paper focuses on the decay of mixed layer near-inertial energy due to the radiation of linear, near-inertial waves. These internal waves are generated by horizontal convergences and divergences in the mixed layer that force the fluid below—a process known as inertial pumping.

Theoretical considerations show that on an f plane the horizontal gradients in the mixed layer are created by the nature of the wind stress forcing. Gill (1982) showed that a moving atmospheric front will generate near-inertial oscillations in its wake. The imposed horizontal scale is a function of the speed of the front and its alongfront structure. A one-dimensional front moving at a speed C forces the mixed layer currents at a horizontal wavenumber $\kappa = f/C$. Linear models developed by Pollard (1970) and Kundu and Thomson (1985) used analytical forms of the wind stress and examined the internal waves created in the wake of the front. Gill (1984) modeled the waves after the storm had passed by initializing the mixed layer with horizontally varying currents—the model then tracks the subsequent wave propagation.

Other modeling efforts include models by Price (1983: multilayered in the vertical, hurricane scales), Rubenstein (1983: multilayered, eddy diffusivity and bottom porosity), Greatbatch (1983, 1984: multilevel ocean, including nonlinearities and entrainment), Kundu (1986: vertical modes with eddy diffusivity), and Shay and Elsberry (1987: hurricane scales, use of vertical modes on a level or sloping bottom). In these cases, the models were two-dimensional and run on an f plane. One common characteristic of the models is that the predicted timescale for mixed layer current decay agrees with observations at small horizontal scales (hurricanes), but not at large scales (atmospheric fronts and propagating storms). For large-scale forcing

Corresponding author address: Dr. Murray D. Levine, College of Oceanic and Atmospheric Sciences, Oregon State University, Oceanography Adm. Bldg. 104, Corvallis, OR 97331-5503.
E-mail: levine@oce.orst.edu

events the predicted decay timescale is larger than observed.

D'Asaro (1989) demonstrated that the β effect causes a reduction of horizontal scales in time, thus accelerating the rate of inertial pumping of energy out of the mixed layer. The meridional wavenumber of the currents will vary as a function of time as $l = l_0 - \beta t$, where l_0 is the initial wavenumber, β the rate of change of Coriolis parameter with latitude, and $l < 0$ denotes propagation to the south. As a result the radiation of energy from the mixed layer increases the pycnocline horizontal kinetic energy (HKE) as t^6 compared with t^2 on an f plane. Although some of the numerical experiments performed by Gill (1984) were on a β plane, more attention was paid to the southward wave propagation than the significance of the effect of the waves on inertial pumping.

The purpose of this paper is to explore further how the wind-generated energy radiates from the mixed layer by the vertical and horizontal propagation of near-inertial waves. Of particular interest is the timescale of the decay of mixed layer energy and the magnitude of the energy transfers to the ocean below. Specifically we want to understand and quantify the energy transfer from the mixed layer as a function of the following initial conditions and background properties:

- initial horizontal wavenumber in the mixed layer (magnitude and direction),
- horizontal extent of the storm,
- mixed layer depth (seasonal stratification), and
- deep stratification.

To study the radiation of energy from the mixed layer we use a linear, numerical model on a midlatitude β plane. The solution is expanded using vertical modes in depth and Fourier transformed in x (zonal); the problem is solved numerically in y (meridional) and time. The results of the model are interpreted in terms of linear wave theory. This comparison of the numerical model with wave theory will permit us to use analytical expressions to predict the timescale and magnitude of the energy leaving the mixed layer as a function of the initial conditions and background properties. Hence, the energy exchange between mixed layer and pycnocline can be described without having to run the numerical model.

We consider our analysis as revisiting the landmark study by Gill (1984, hereafter referred to as G84). As in G84, we distribute the wind-generated current, initially concentrated within the mixed layer, into vertical modes, and then let the modes propagate horizontally as free waves. Phase differences between the modes develop as each mode oscillates at a discrete frequency. The wave field, which is the sum of all the modes, evolves from the initial condition and develops nonzero velocities below the mixed layer. As a result, we have propagation of energy with depth. The horizontal propagation of each mode is treated numerically in the meridional direction and spectrally in the zonal.

The model in G84 has been modified to determine the effect of the initial conditions and background properties on the wave propagation. We have added the zonal dimension to the model and determined under what conditions this dimension is important. The initial condition of mixed layer velocity has been altered to represent a velocity field consistent with a propagating front; the G84 initial conditions are not compatible with this forcing. The effect of a limited north–south extent of the forcing is addressed explicitly.

As with all models, some potentially important physical processes have been neglected, most notably nonlinear dynamics and viscosity. Probably much of the behavior of the near-inertial wave field can be explained with linear dynamics; it is certainly the logical starting point. Failure of the model to explain observed features will suggest which omitted processes may be important.

This study is motivated by the observations made during the Ocean Storms Experiment in the northeast Pacific Ocean (D'Asaro et al. 1995). Several strong storm events generated significant near-inertial oscillations in the mixed layer that could be tracked for weeks as they propagated vertically into the pycnocline. The analysis here provides a framework for interpreting these data—the application to the Ocean Storms data is found in the companion paper Levine and Zervakis (1995).

The numerical model is presented in section 2. Linear wave dynamics are discussed in section 3 to provide a basis for interpreting the model results. The model results are shown in section 4, demonstrating the dependence of the decay timescale on the initial conditions and background properties; comparison is made with the behavior of analytical wave theory. A summary and conclusions are given in section 5.

2. Model formulation

The model of near-inertial waves is patterned after the model developed by G84 with some important differences. The model is based on the momentum equations for a linear, inviscid, Boussinesq ocean given by

$$\frac{\partial u}{\partial t} - fv = -\frac{\partial p}{\partial x} \tag{1}$$

$$\frac{\partial v}{\partial t} + fu = -\frac{\partial p}{\partial y} \tag{2}$$

$$0 = -\frac{\partial p}{\partial z} - g\frac{\rho'}{\rho_0}, \tag{3}$$

where x, y, and z denote the zonal, meridional, and vertical axes, increasing to the east, north, and upward from the ocean bottom respectively; u, v, w are the components of the velocity in the x, y, z directions; f

is the latitude-dependent Coriolis parameter; and the density has been decomposed into a constant ρ_0, a mean density profile $\rho_1(z)$, and a perturbation density $\rho'(x, y, z, t)$. The pressure p has been normalized by ρ_0, consistent with G84. The hydrostatic approximation has been adopted in the vertical momentum balance. The ocean is assumed incompressible:

$$\frac{\partial u}{\partial x} + \frac{\partial v}{\partial y} + \frac{\partial w}{\partial z} = 0, \tag{4}$$

and mass continuity is given by

$$\frac{g}{\rho_0}\frac{\partial \rho'}{\partial t} - N^2 w = 0, \tag{5}$$

where N is the buoyancy frequency defined by $N^2 = -g/\rho_0(d\rho_1/dz)$ in which g is the acceleration of gravity.

Eliminating ρ' and w by substituting (3) and (5) into (4), we retrieve a system of three coupled equations in three variables, u, v, and p. Since the equations are first order in time, the initial conditions can be written:

$$[u(x, y, z, t), v(x, y, z, t)]_{t=0} = [u^i(x, y), v^i(x, y)]S(z)$$
$$[p(x, y, z, t)]_{t=0} = p^i(x, y)S(z), \tag{6}$$

where $S(z)$ is defined to limit the initial currents to the mixed layer:

$$S(z) \equiv \begin{cases} 1, & H - H_{\text{mix}} < z < H \\ 0, & 0 < z < H - H_{\text{mix}}, \end{cases} \tag{7}$$

where H_{mix} is the mixed layer depth, $z = 0$ is the ocean bottom, and $z = H$ is the surface. The above formulation assumes that the mixed layer depth is constant and the direct effect of the wind does not extend below the mixed layer.

The vertical dependence of u, v, w, and p is represented by an expansion into vertical modes:

$$(u, v, p) = \sum_{n=0}^{\infty} \sigma_n(\tilde{u}_n, \tilde{v}_n, \tilde{p}_n)\phi_n(z) \tag{8}$$

$$w = \sum_{n=1}^{\infty} \tilde{w}_n\psi_n(z), \tag{9}$$

where the wave functions ψ_n and ϕ_n are eigenfunctions of

$$\frac{d}{dz}\left(\frac{1}{N^2(z)}\frac{d\phi_n}{dz}\right) + \frac{1}{c_n^2}\phi_n = 0 \tag{10}$$

$$\frac{d^2\psi_n}{dz^2} + \frac{N^2(z)}{c_n^2}\psi_n = 0 \tag{11}$$

and c_n^{-2} are the eigenvalues; a rigid-lid boundary condition [$\psi_n(0) = 0$, $\psi_n(H) = 0$] is assumed. We will refer to c_n as *modal eigenspeeds,* as they are not phase speeds. The eigenspeeds have units of velocity, are a function of stratification and ocean depth only, and define the minimum phase speed and maximum horizontal group speed of each vertical normal mode (Kundu 1993). The barotropic mode is neglected since $c_0 \gg c_1$ (virtually instantaneous adjustment), and the barotropic currents are weak (Gill 1982).

For convenience we keep the normalization as in G84, so that

$$\phi_n(H) = 1, \tag{12}$$

and the weights σ_n are defined by the modal expansion of $S(z)$:

$$S(z) = \sum_{n=0}^{\infty} \sigma_n\phi_n(z). \tag{13}$$

Then, σ_n denotes the contribution of each mode to the initial velocity in the mixed layer, while the horizontal and temporal variation of the wave field is controlled by the modal coefficients $\tilde{u}_n$, $\tilde{v}_n$, $\tilde{p}_n$, and $\tilde{w}_n$, which are functions of x, y, and t. It is convenient to represent the zonal variations (x dependence) of $\tilde{u}_n$, $\tilde{v}_n$, $\tilde{w}_n$, and $\tilde{p}_n$ by a Fourier transform:

$$(\hat{u}_n, \hat{v}_n, \hat{w}_n, \hat{p}_n) = \int_{-\infty}^{+\infty} (\tilde{u}_n, \tilde{v}_n, \tilde{w}_n, \tilde{p}_n)e^{-ikx}dx, \tag{14}$$

where the caret identifier denotes functions of (k, y, t). After substituting the modal expansions (8) and (9) into (1)–(5), Fourier transforming in x (14), and eliminating $\hat{w}_n$ and $\hat{p}_n$, we retrieve two coupled equations in (u, v) that govern the horizontal propagation of mode n:

$$\frac{\partial^2\hat{u}_n}{\partial t^2} - f\frac{\partial\hat{v}_n}{\partial t} = -c_n^2k^2\hat{u}_n + ic_n^2k\frac{\partial\hat{v}_n}{\partial y} \tag{15}$$

$$\frac{\partial^2\hat{v}_n}{\partial t^2} + f\frac{\partial\hat{u}_n}{\partial t} = +c_n^2\frac{\partial^2\hat{v}_n}{\partial y^2} + ic_n^2k\frac{\partial\hat{u}_n}{\partial y}. \tag{16}$$

The system is now fourth order in time and requires four initial conditions (of which three are independent) that can be written in terms of u^i, v^i, and p^i (6):

$$[\hat{u}_n, \hat{v}_n]_{t=0} = \int_{-\infty}^{\infty} [u^i, v^i]e^{-ikx}dx$$

$$\left[\frac{\partial\hat{u}_n}{\partial t}, \frac{\partial\hat{v}_n}{\partial t}\right]_{t=0} = \int_{-\infty}^{\infty}\left[\left(fv^i - \frac{\partial p^i}{\partial x}\right), \left(-fu^i - \frac{\partial p^i}{\partial y}\right)\right]e^{-ikx}dx. \tag{17}$$

Note that the initial conditions are the same for each mode.

It is assumed that the horizontal structure of the initial condition is determined by the speed and direction of the atmospheric front; the model then tracks the oce-

anic response after the wind has imparted a velocity field into the mixed layer. The form of the initial condition is based on results from previous analyses of the mixed layer response to an infinite front moving with a finite speed (e.g., Gill 1982; Kundu and Thomson 1985). The solution can be described for each baroclinic mode in terms of the advection speed C of the storm and the eigenspeed c_n of the mode. When $C < c_n$, the equation governing the horizontal radiation of the mode is elliptical, and the solution decays exponentially from the center of the storm. When the storm is fast, $C > c_n$, the equation is hyperbolic, and the solution is a wake of near-inertial oscillations propagating behind the forcing. In the latter case, the mixed layer inertial oscillations develop a horizontal wavenumber $\kappa = f_0/C$, where f_0 is the local inertial frequency. The quantity $2\pi/\kappa$ is called the "inertial wavelength" by Kundu and Thomson (1985), and D'Asaro (1989) calls $1/\kappa$ the "advection scale" of the storm. We assume that the storm is fast relative to c_1, and since $c_1 > c_n$, the storm is faster than all modes. Therefore, we choose the initial mixed layer current to have the form of a pure inertial oscillation:

$$[u^i, v^i]_{t=0} = U_0 L(y)[\cos(k_0 x + l_0 y - f_0 t), \sin(k_0 x + l_0 y - f_0 t)]|_{t=0}$$

$$[p^i]_{t=0} = 0, \tag{18}$$

where (k_0, l_0) is the horizontal wavenumber in the direction of C and $\kappa \equiv (k_0^2 + l_0^2)^{1/2}$. The function $L(y)$ is a smooth, slowly varying function that limits the north–south extent of the initial disturbance (Fig. 1). This function models the weakening of a propagating front. No limit is yet specified in the east–west direction. The amplitude U_0 depends on the strength of the wind and depth of the mixed layer; the detailed analysis of the momentum transfer from the wind to the mixed layer can be found elsewhere (e.g., Gill 1982; Kundu and Thompson 1985). Since the main objective of this paper is to follow the near-inertial wave propagation after the storm has passed, we leave U_0 as an arbitrary parameter.

Note that the initial condition introduced above is considerably different than the one used by G84:

$$[u^i(y), v^i(y)]_{t=0} = U_0 L(y)[\sin(l_0 y), 0]$$

$$\left[\frac{\partial u^i}{\partial t}, \frac{\partial v^i}{\partial t}\right]_{t=0} = [0, 0]. \tag{19}$$

In this formulation $k_0 = 0$, but the fundamental difference is that this initial condition is not consistent with inertial currents generated by a moving front. This velocity field has the structure of two waves: one propagating northward and one southward, that is, a standing wave. Also, G84 adopted two values of horizontal extent: $L(y) = \infty$ and $L(y) = 2\pi l_0^{-1}$ (one wavelength). In the present study $L(y)$ is a parameter independent of l_0.

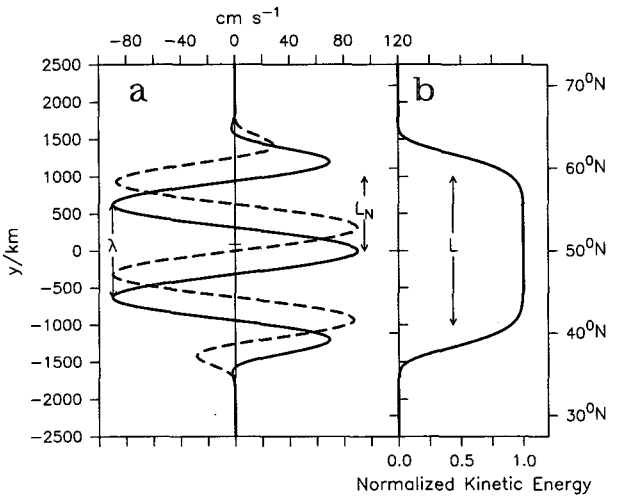

FIG. 1. (a) Example of initial conditions u^i (solid line), v^i (dashed line) as a function of latitude, with a meridional wavelength $\lambda = 2\pi l_0^{-1} \approx 628$ km and a northern extent $L_N = 1000$ km. (b) The normalized HKE of the initial condition, as a function of latitude. Latitude scale is given in both degrees and kilometers.

Using (18), the Fourier transformed initial conditions (17) for mode n become

$$\hat{u}_n|_{t=0} = \frac{U_0 L(y)}{2} \times \{[\delta(k - k_0) + \delta(k + k_0)]\cos(l_0 y - f_0 t) + i[\delta(k - k_0) - \delta(k + k_0)] \times \sin(l_o y - f_0 t)\}|_{t=0}$$

$$\hat{v}_n|_{t=0} = \frac{U_0 L(y)}{2} \times \{[\delta(k - k_0) + \delta(k + k_0)]\sin(l_0 y - f_0 t) - i[\delta(k - k_0) - \delta(k + k_0)] \times \cos(l_o y - f_0 t)\}|_{t=0}$$

$$\left.\frac{\partial \hat{u}_n}{\partial t}\right|_{t=0} = \frac{f U_0 L(y)}{2} \times \{[\delta(k - k_0) + \delta(k + k_0)]\sin(l_0 y - f_0 t) + i[\delta(k - k_0) - \delta(k + k_0)] \times \cos(l_o y - f_0 t)\}|_{t=0}$$

$$\left.\frac{\partial \hat{v}_n}{\partial t}\right|_{t=0} = \frac{-f U_0 L(y)}{2} \times \{[\delta(k - k_0) + \delta(k + k_0)]\cos(l_0 y - f_0 t) - i[\delta(k - k_0) - \delta(k + k_0)] \times \sin(l_o y - f_0 t)\}|_{t=0}, \tag{20}$$

where $\delta(k)$ is the Kronecker delta.

Equations (15) and (16) with the initial conditions (20) are solved numerically in y and t using finite differences. The spatial resolution was 10 km and the time step was 10 min. Typically 30 modes were used: tests showed that using more modes made a negligible difference. The domain extended 2500 km north and south of the central latitude ($y = 0$). The extent to the north provides ample space for the initially northward propagating waves to reach their turning latitude and turn to the south (Anderson and Gill 1979); thus, no special boundary condition was needed on the northern limit of the domain. At the southern boundary, we incorporated a sponge layer; a body friction term was added to (15) and (16) with a friction coefficient $r_0(y)$ increasing linearly from 0 at $y = -2000$ km to a value determined by trial and error, at $y = 2500$ km. The slope dr_0/dy was determined by minimizing the waves reflected back from the southern boundary. Without a sponge layer at the southern boundary Anderson and Gill (1979) demonstrated clearly that waves are reflected northward and create interference patterns with the southward propagating waves. The optimal solution would be the adoption of an absorbing boundary condition instead of a sponge layer. Such a condition has been proposed by Higdon (1994) for a wave equation similar to (15)–(16); however, it requires an estimate of the phase speed of the waves. In the present case, the phase speed is time varying and mode dependent, so the phase speed would have to be estimated at every time step and for each mode, which is quite complicated and computationally expensive.

3. Theoretical considerations

Before solving the initial value problem numerically, it is useful to consider the basic concepts of horizontal and vertical wave propagation expressed as a sum of vertical modes. These ideas will be valuable in interpreting the numerical solutions and will provide insight into the dependence of the evolution of the wave field on the initial conditions (wavenumber and horizontal extent) and the background properties (mixed layer depth and stratification).

a. Dispersion relation

We can anticipate the numerical model results by using ray theory to track the horizontal propagation of vertical modes. To apply ray theory we assume that the horizontal dependence of the amplitude of a mode can be expressed in the form $\exp[i(kx + ly - \omega t)]$; that is, each mode can be expressed as a horizontally propagating plane wave with slowly varying wavenumber and frequency. Substitution into (15) and (16) yields a fourth-order polynomial for the frequency ω; one root, $\omega = 0$, is artificial, introduced by the increase of the system to fourth order; the second root describes the vortical mode on an f plane or a Rossby planetary wave on a β plane. The two remaining roots of the characteristic polynomial are the solutions of the dispersion relation for each mode:

$$\omega_n^2 = f^2 + c_n^2(k^2 + l^2), \tag{21}$$

which is the same relation as for internal Poincaré waves. The near-inertial internal gravity waves following (21) will have a much stronger response to the initial conditions (18) than the Rossby wave solution.

It proves convenient to define at this point a dimensionless parameter ϵ by

$$\epsilon \equiv \frac{c_n^2(k^2 + l^2)}{f^2}. \tag{22}$$

It can be shown that ϵ is equivalent to the square of the ratio of the Rossby radius to the horizontal scale ($1/\kappa$) of the waves, where the Rossby radius is defined as the minimum phase speed c_n divided by f (Gill 1984). Although ϵ is time and mode dependent, it is, in general, less than 0.05 for typical midlatitude conditions. Note that ϵ increases toward the equator.

Using the dispersion relation (21), the ray equations become (e.g., Lighthill 1978)

$$\frac{dx}{dt} = \frac{\partial \omega_n}{\partial k} \quad (\equiv C_{gn}^x)$$

$$= \frac{c_n^2 k}{f}(1 + \epsilon)^{-1/2} \tag{23}$$

$$\frac{dy}{dt} = \frac{\partial \omega_n}{\partial l} \quad (\equiv C_{gn}^y)$$

$$= \frac{c_n^2 l}{f}(1 + \epsilon)^{-1/2} \tag{24}$$

$$\frac{dk}{dt} = -\frac{\partial \omega_n}{\partial x} = 0 \tag{25}$$

$$\frac{dl}{dt} = -\frac{\partial \omega_n}{\partial y} = -\beta(1 + \epsilon)^{-1/2}, \tag{26}$$

where $\beta \equiv df/dy$. These equations define the ray path along which the energy in each mode propagates as well as the wavenumber changes along that ray. Since the dispersion relation is not a function of t or x, then ω and k are invariant along a ray. Due to the β effect the north–south wavenumber varies as the wave propagates along the ray for small ϵ (26) as

$$l(t) = l_0 - \beta t. \tag{27}$$

For an initial wavenumber $l_0 < 0$ (southward propagation), the *magnitude* of l increases linearly in time; for $l_0 > 0$ (northward propagation), the magnitude initially decreases, goes through zero, and finally increases, linearly in time. As a result of the time dependence of the meridional wavenumber, the rays are curved (Fig. 2). A northward ray eventually reaches its turning latitude and turns to the south (Fig. 2a),

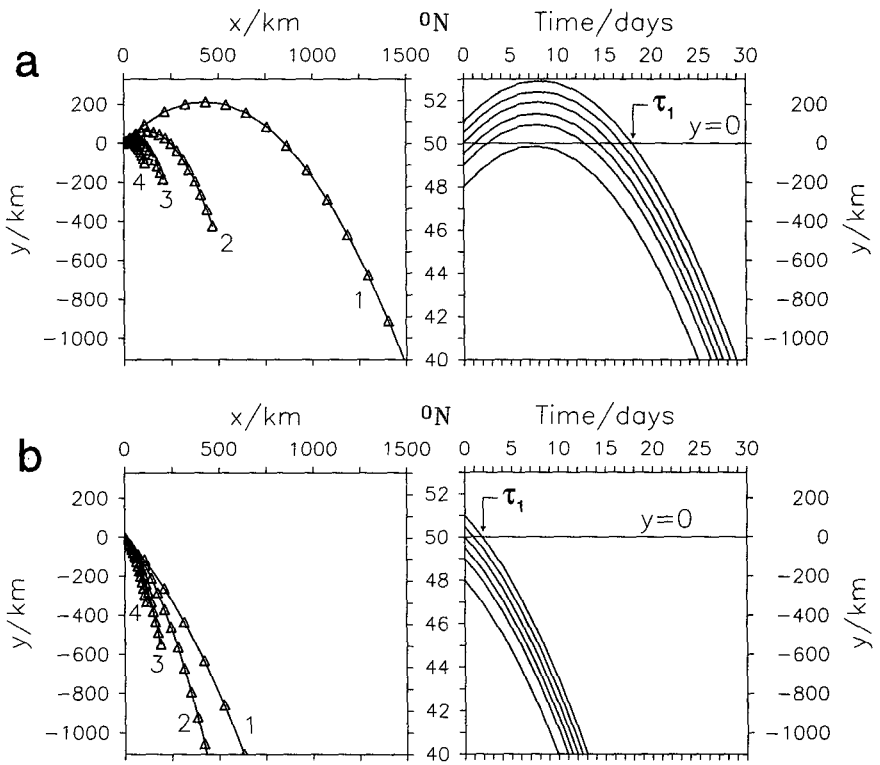

FIG. 2. Example of ray paths for initial wavenumber (k_0, l_0) of (a) a northward propagating wave (0.01, 0.01) and (b) a southward propagating wave (0.01, −0.01). The panels on the left display the ray paths of the lowest four modes, starting at $y = 0$, as a function of latitude and longitude. Paths are plotted for no more than 30 days; a mark is plotted on the ray every two days. Note that the very low modes travel very fast and soon leave the generation area; the higher modes effectively remain where they were forced. The right panels display the ray paths on a latitude–time plane of mode 1 that starts from different values of y. Note that it is always the northernmost ray that is the last to leave the observation point $y = 0$ (in this case, 50°N) at τ_1.

while a southward ray keeps turning more southward until it crosses the equator (Fig. 2b).

Note that for small ϵ, the components of the group velocity, C^x_{gn} and C^y_{gn}, are functions only of the wavenumber component that is in the same direction, k and l, respectively. Hence, for small ϵ the meridional wavenumber does not have any effect on the zonal propagation of the waves, and vice versa. Also, for small values of ϵ, the dispersion relation (21) can be written approximately in simpler form:

$$\omega_n = f\left(1 + \frac{\epsilon}{2} + \cdots\right) \approx f + \frac{c_n^2(k^2 + l^2)}{2f}. \quad (28)$$

b. *Modal interference (beating)*

Gill (1984) explains in detail how the vertical propagation of near-inertial energy is expressed as a sum of vertical modes at a fixed location. Initially the sum of the modes matches the function $S(z)$, a constant value in the mixed layer and zero below. In this problem all modes have the same initial horizontal wavenumber (k_0, l_0). In addition for all modes $k = k_0$ is constant in time, while l changes in time as given in (27). Since $c_1 > c_2 > c_3 > \cdots$, the lower the mode the higher its frequency (21). The frequency of the high modes is very nearly f_0 because c_n goes to 0 as $n \to \infty$. Since each mode oscillates at a slightly different frequency, their relative phase is constantly changing in time. G84 defines as t_n the time when mode n will become out of phase with the high modes at frequencies near f_0:

$$t_n = \frac{\pi}{(\omega_n - f_0)}. \quad (29)$$

At time t_1, mode 1 will add destructively to the other modes in the mixed layer, and the sum of the modes below the mixed layer will no longer be zero. Thus, we will observe vertical propagation of energy from the mixed layer into the pycnocline. At time t_2, mode 2 will be out of phase with the high modes and more energy will have propagated into the pycnocline. However, this reasoning is oversimplified, since by time t_2 mode 1 may again be enforcing the mixed layer currents again. Nonetheless, energy exchanges between the mixed layer and the pycnocline, called inertial beat-

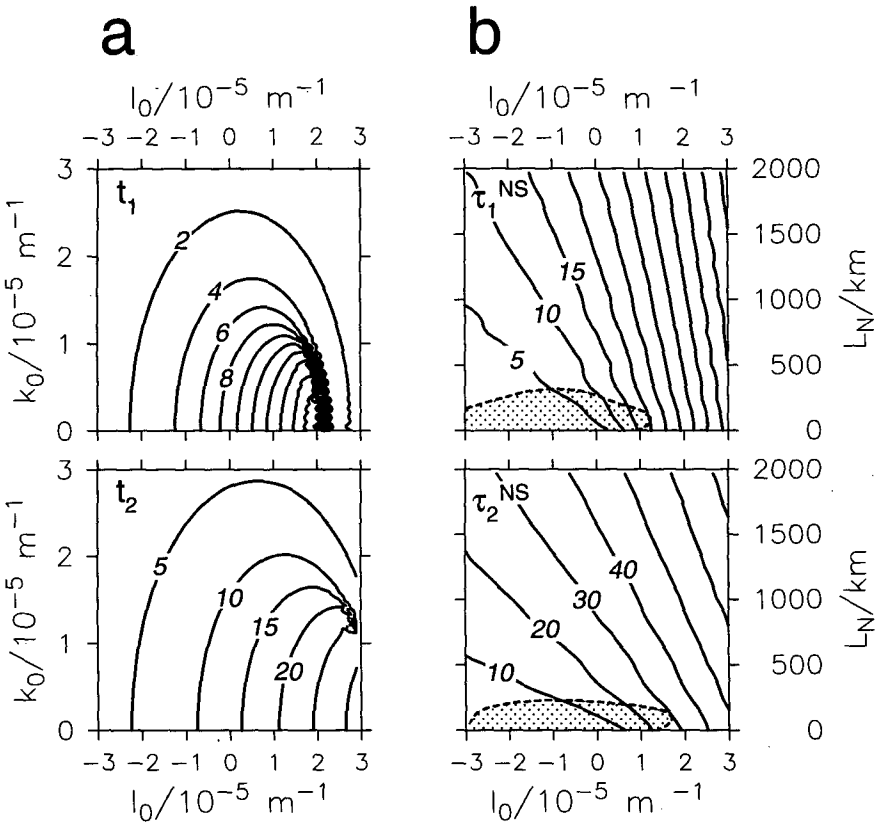

FIG. 3. Contours in days of the timescales (a) t_n and (b) τ_n^{NS} for $n = 1$ and 2, for the stratification profile defined by Eq. (35), with $H_{mix} = 150$ m at 50°N. Note: t_n is plotted as a function of initial wavenumber (k_0, l_0); τ_n^{NS} is plotted as a function of initial wavenumber l_0 and northern extent L_N for $k_0 = 0$. The shaded areas of (b) represent the parameter range where $\tau_n^{NS} < t_n$; that is, mode n will have propagated away before beating can occur.

ing, can be explained as a result of the interference of vertical modes, and the timescales for these exchanges are determined by the frequency differences between the modes. On an f plane the timescale t_n is easily calculated since ω_n is constant.

Here, we incorporate β-plane geometry into the definition of t_n (29). Using (27) and (28), ω_n is now a function of time:

$$\omega_n \approx f_0 + \frac{c_n^2[k_0^2 + (l_0 - \beta t)^2]}{2f_0}. \qquad (30)$$

Note that this frequency, observed at $y = 0$, changes in time, while the frequency following a ray is constant. This is because the waves observed at $y = 0$ continually come from different ray paths. For an Eulerian observer, $f = f_0$ (a constant) and ω_n varies in time; for an observer moving along a ray, $f = f(y)$ and ω_n is a constant. In the present context we analyze the model results from an Eulerian viewpoint, and thus we use f_0 in (21) and equations derived from it. Substituting (30) into (29), we get a cubic equation for t_n:

$$t_n^3 - \frac{2l_0}{\beta} t_n^2 + \frac{k_0^2 + l_0^2}{\beta^2} t_n - \frac{2f_0\pi}{c_n^2\beta^2} = 0, \qquad (31)$$

which has three roots. The smallest, positive, real root defines the t_n of interest, that is, the first time at which mode n will be out of phase with f_0. Figure 3a shows values for t_1 and t_2 as a function of k_0 and l_0 using $c_1 = 2.8$ m s^{-1} and $c_2 = 1.9$ m s^{-1} for $H_{mix} = 150$ m and typical midlatitude deep stratification. Note that the largest value of $t_1 \sim 20$ days is found at $k_0 = 0$, $l_0 = 1.5 \times 10^{-5}$ m^{-1}, which corresponds to a northward moving storm. Also note that at high wavenumbers the asymmetry between northward and southward propagating waves due to the β effect tends to decrease.

c. *Modal departure due to north–south propagation*

Ray theory can be used to understand the effect of a finite north–south extent of the initial disturbance. On a β plane the energy of each mode propagates meridionally at the group velocity (24) given by

$$\frac{dy}{dt} = \frac{c_n^2 l}{f} = \frac{c_n^2(l_0 - \beta t)}{f} \qquad (32)$$

for small ϵ. The group velocity can be used to compute the time it takes for the energy in a mode to propagate meridionally between two points. The time τ it takes for a mode to travel from $y = y_0$ to $y = 0$ is obtained by integrating (32) using $f = f_0 + \beta y$ and solving explicitly for τ:

$$\tau^2 - \frac{2l_0}{\beta}\tau - \left[\frac{2f_0y_0 + \beta y_0^2}{c_n^2\beta}\right] = 0. \qquad (33)$$

In the case of initially southward propagating waves ($l_0 < 0$), there is one positive root for $y_0 > 0$; there are no real roots for $y_0 < 0$, as the wave never reaches $y = 0$ (Fig. 2b). For northward propagating waves ($l_0 > 0$) there are two positive roots when

$$y_0 > -d_{\text{crit}} \equiv -\frac{c_n^2 l_0^2}{2f_0\beta}, \qquad (34)$$

(where d_{crit} is the northward distance a ray travels before turning) representing the two times the ray crosses $y = 0$ (Fig. 2a). At the first crossing the wave is propagating northward and at the second it is propagating southward after reflecting at the turning latitude. Waves starting at $y_0 < -d_{\text{crit}}$ never reach $y = 0$. Based on the above modal propagation estimates, we can determine the duration for which a mode will be present at $y = 0$. We define τ_n^{NS} as the time when all the energy at mode n initially to the north or south of $y = 0$ will have propagated away and will no longer contribute to the wave field at $y = 0$. Figure 2 clearly demonstrates that it is always the ray that starts from the northernmost point that is the last to leave the point $y = 0$, independent of the propagation direction of the initial wave. By replacing y_0 by L_{N} in (33), we can calculate the time τ_n^{NS} after which all the energy of mode n will have propagated away from $y = 0$, never to return.

Clearly, τ_n^{NS} is a function of l_0 and the northern extent L_{N}. As an example, the time τ_n^{NS} is contoured in units of days as a function of initial wavenumber l_0 and northern extent L_{N} for typical midlatitude stratification with $H_{\text{mix}} = 150$ m and $k_0 = 0$ (Fig. 3b).

d. Modal departure due to east–west propagation

Determining the effect of an initial finite east–west extent is simpler than a north–south extent, since C_{gn}^x is constant in time for small ϵ. Let the initial east and west extent from $x = 0$ be L_{E} and L_{W}. For an eastward propagating wave ($k_0 > 0$), the propagation time τ_n^{EW} for a mode to go from $x = L_{\text{W}}$ to $x = 0$ is given by

$$\tau_n^{\text{EW}} \equiv \frac{L_w}{C_{g_n}^x} = \frac{f_0 L_w}{c_n^2 k_0}. \qquad (35)$$

After time τ_n^{EW} mode n will no longer contribute to the solution at $x = 0$. For a westward propagating wave, τ_n^{EW} is also given by (35) after replacing L_{W} by L_{E}.

e. Comparing the timescales

The timescales of inertial beating t_n and the timescales of propagation τ_n^{NS} and τ_n^{EW} are useful concepts that help in understanding the results of the numerical model. Both of these timescales are functions of the modal eigenspeed c_n that depends on the stratification and ocean depth. If τ_n^{NS} or τ_n^{EW} are smaller than t_n, then mode n will have propagated away horizontally before the effect of inertial beating involving that mode would be observed (Fig. 3b).

To summarize the meridional propagation of the modes and their relative phase difference, we introduce Fig. 4. The phase difference $\Delta\phi_n = (\omega_n - f)t$ between the seven lowest modes and a perfect inertial current, representative of high modes, is plotted as a function of time. Solid horizontal lines are drawn at π and 3π, where the low modes add destructively to the high modes; dashed lines are drawn at 2π and 4π, where the modes interfere constructively. The time t_n is defined as the time the phase reaches π. Superimposed on the phase plots are the estimated times τ_n^{NS}, where all the energy of a mode will have departed, for various values of L_{N}. All the estimates were made for $(k_0, l_0) = (0, 0)$. For example, for a small northern extent of 250 km, we expect that the first mode will propagate away before beating with f_0, while the second mode will barely have time to beat before leaving. On the contrary, for a large northern extent of 1500 km, mode 1 will add constructively and destructively many times before leaving.

4. Model results

The numerical model was run to determine the radiation of near-inertial motion from the mixed layer for

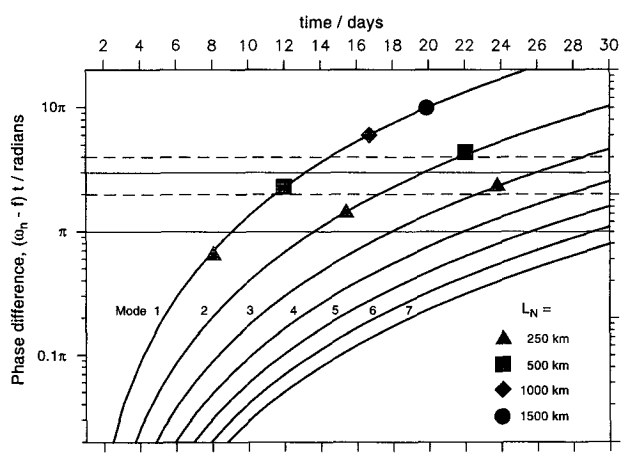

FIG. 4. Phase difference of the seven lowest modes with a perfectly inertial current, as a function of time with $(k_0, l_0) = (0, 0)$. Note that while all modes start in phase, significant phase differences develop. The intersection with the line denoting a phase difference π defines the timescale t_n. Overlaid on the phase plots are estimates of the timescale τ_n^{NS}, when a mode will have left the area, for different values of northern extent L_{N}.

a range of initial conditions (horizontal wavenumber, north–south extent) and background properties (stratification, mixed layer depth). The effect of one factor on the near-inertial propagation is not independent of the others; however, some notion of the model behavior can be obtained from a small number of model experiments. The model results are interpreted with the aid of the wave concepts discussed in section 3. This promotes a physical understanding of the model and will permit us to predict model results without actually running the numerical model.

We chose a stratification profile used in G84 given by

$$N(z) = \begin{cases} \dfrac{s_0}{H + H_{\text{virt}} - z}, & z < H - H_{\text{mix}} \\ 0, & z \geq H - H_{\text{mix}}, \end{cases} \tag{36}$$

where $s_0 = 2.5$ m s^{-1} and $H_{\text{virt}} \equiv s_0/N_0 - H_{\text{mix}}$. This profile has a peak N_0 at the base of the mixed layer, and s_0 is chosen to fit a typical ocean profile. This idealized $N(z)$ is compared with historical data from the Pacific and Atlantic Oceans in Fig. 5. Profiles of the idealized $N(z)$ for a variety of mixed layer depths are shown in Fig. 6 with the corresponding values of σ_n and c_n. The dependence of the wave propagation on the seasonal (mixed layer depth) and deep stratification are considered hereafter.

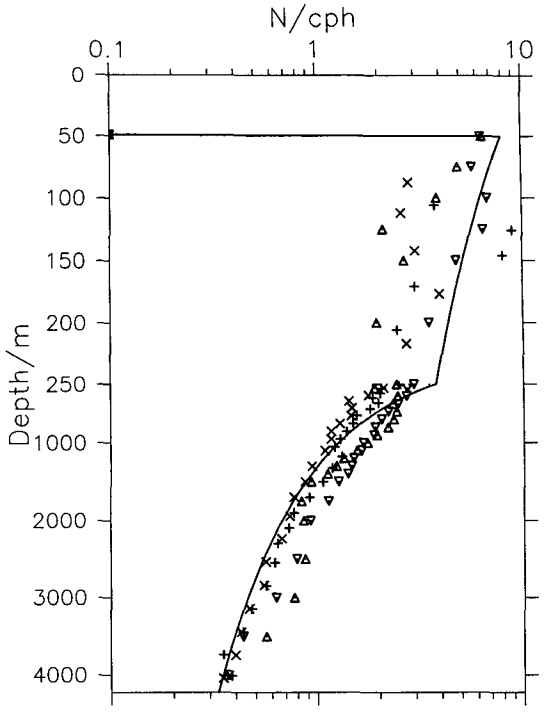

FIG. 5. The idealized buoyancy frequency profile (solid line) defined by Eq. (36). Shown for comparison are two zonally averaged profiles (Levitus 1982) from the North Atlantic (△) and the Pacific (▽) Oceans as well as two individual CTD casts from the North Pacific Ocean (+, from 47.0°N, 135.7°W, and ×, from 47.0°N, 171.6°E). Note the change of scale of the vertical axis at 250-m depth.

a. Model experiments: f versus β plane

Sample results of model experiments on an f and β plane are shown in Fig. 7. In these runs $L = 3000$ km and $H_{\text{mix}} = 100$ m. The initial wavenumber is consistent with a storm front moving southward at 20 m s^{-1}; that is, $l_0 \approx -2.5 \times 10^{-6}$ m^{-1} $= (-400$ km$)^{-1}$ and $k_0 = 0$. At $y = 0$ (50°N), the vertically integrated horizontal kinetic energy (HKE) over the entire depth E_T (0 to 4000 m), the mixed layer E_{ML} (0 to H_{mix}), and the pycnocline E_{PC} (H_{mix} to H_{mix} + 200 m) are shown in the upper panels (Fig. 7). The middle panels display the u component of velocity in the mixed layer as a function of latitude and time. The modeled currents were complex demodulated around f_0, using a boxcar window four inertial periods long. The phase was back-rotated in time at the local inertial frequency f_0.

On an f plane, the initial wavenumber l_0 is too small for effective inertial pumping (Fig. 7a). Hence E_{ML} decreases slowly during the first 30 days while l remains constant. The decrease in E_{ML} is primarily due to the vertical propagation into the pycnocline as E_T remains relatively constant. The theoretical timescale, $t_1 = 35$ days, for inertial beating is consistent with the numerical model decrease in E_{ML}. That the north–south extent is finite is not important in this case as τ_1^{NS} is much greater than t_1: the waves propagate southward, but very slowly.

On the β plane (Fig. 7b) smaller scales develop in time as suggested by theory (27). Note that inertial pumping increases as the horizontal scale decreases. By day 10 the horizontal scale has decreased to 100 km (wavelength of 600 km) and much of the energy has left the mixed layer. This decrease in E_{ML} occurs around time t_1 and can be explained by the beating (destructive interference) of mode 1 with the other modes. At this time E_{PC} increases, indicating vertical propagation of energy into the pycnocline, largely due to the contribution from mode 1. By day 13 there appears to be an exchange of energy from the pycnocline back to the mixed layer. This phenomena is reminiscent of the explanation in G84 for an f plane when mode 1 again becomes in phase with f_0. However, here on a β plane the phase of mode 1 is increasing at an ever increasing rate $\sim t^3$ and the phase has already reached 4π by day 13. Hence, explaining this subsequent oscillation of energy back into the mixed layer is not possible using this simple argument. Here E_T remains about the same until day 17; the decrease in E_T occurs at time τ_1^{NS} when the final contribution to mode 1 from 1500 km to the north has propagated away from $y = 0$, never to return.

The bottom panels of Fig. 7 display the inertial currents at $y = 0$ as they evolve with depth and time;

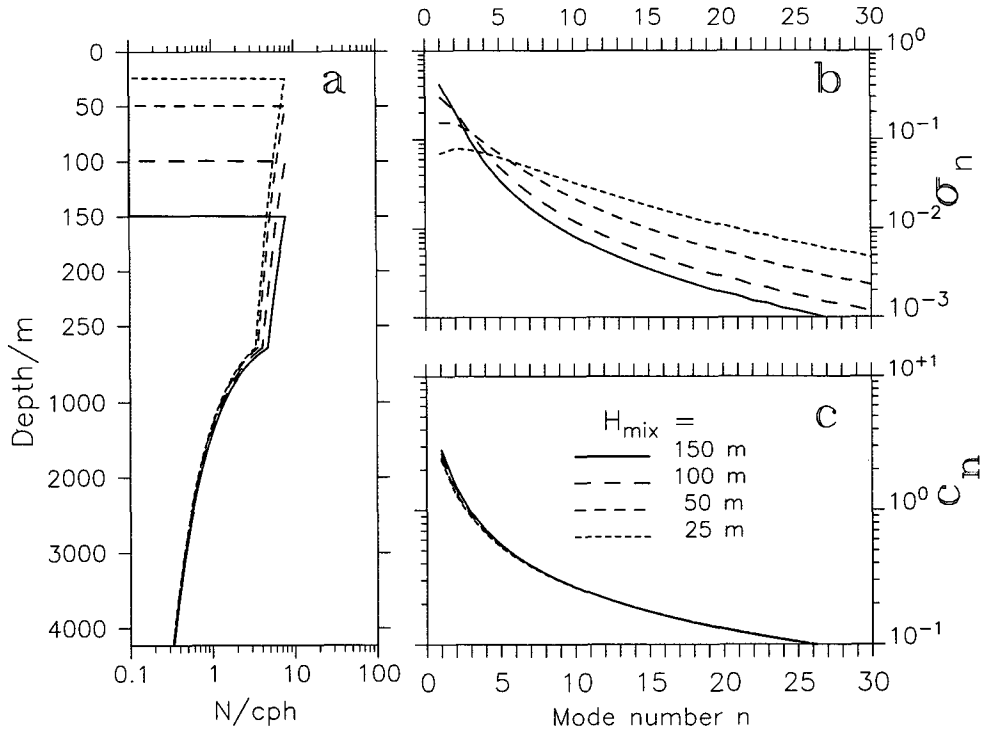

FIG. 6. (a) Idealized profiles of buoyancy frequency as defined by Eq. (36) for various mixed layer depths. The corresponding values of (b) modal coefficient σ_n and (c) modal eigenspeed c_n are plotted as a function of mode number. Note that while variations in the mixed layer depth have a strong effect on σ_n, values of c_n are virtually unchanged.

contours of amplitude are superimposed on the current vectors at selected depths, backrotated at f_0. Although the currents propagate vertically from the mixed layer downward, E_{PC} is concentrated within the top 40 meters of the pycnocline (100–140 m) in both f and β planes. However, in the β plane a larger fraction of the HKE penetrates into the deep ocean by day 30. In fact, at times when $E_{ML} \approx 0$, the HKE is approximately equally divided between E_{PC} and the deep water.

As the current vectors have been inertially backrotated, a change in direction denotes a frequency different from f_0. On an f plane at a constant depth, the current vectors rotate very slowly and monotonically clockwise in time, which indicates that the frequency is slightly superinertial. However, on a β plane the current vectors rotate faster (mostly clockwise), denoting a higher frequency. The current in the mixed layer is homogeneous; there is a significant phase jump across the base of the mixed layer. At times when the amplitude is a minimum in the mixed layer, subinertial frequencies can be identified for a couple of inertial periods. In the β plane the currents at depth between 140 and 1000 m are mostly in phase, while the phase seems to change sign below 2000 m; this pattern suggests the dominance of low modes in determining the deep wave field.

b. *Understanding the model results: Comparison with analytical predictions*

The model results of vertically integrated HKE as a function of depth and time for L_N = 250, 500, and 1000 km and H_{mix} = 25, 50, 100, and 150 m are shown in Fig. 8. The initial HKE in J m^{-2}/m of mixed layer is the same for each value of H_{mix}. The initial wavenumber in the top four rows is consistent with a storm front moving southward at 15 m s^{-1} ($k_0 = 0$, $l_0 = -0.75 \times 10^{-5}$ m^{-1}). In the last row, the initial wavenumber is set by a storm propagating northward at the same speed ($k_0 = 0$, $l_0 = +0.75 \times 10^{-5}$ m^{-1}). The corresponding relative phases, backrotated at frequency f_0, are shown as a function of time at various depths in Fig. 9.

The decrease in E_T can be attributed to horizontal propagation (Fig. 8). The larger the northern extent L_N, the longer the time a given mode will contribute at $y = 0$. The analytical predictions of timescales τ_1^{NS} as calculated from (33) are also indicated in Fig. 8. For a given H_{mix}, the decay of the total HKE is faster when the northern extent L_N is smaller. The first decrease in E_T is coincident with τ_1^{NS}; this is consistent with the idea that mode 1 has left $y = 0$ heading south. For the smaller extents mode 2 may also leave within the first

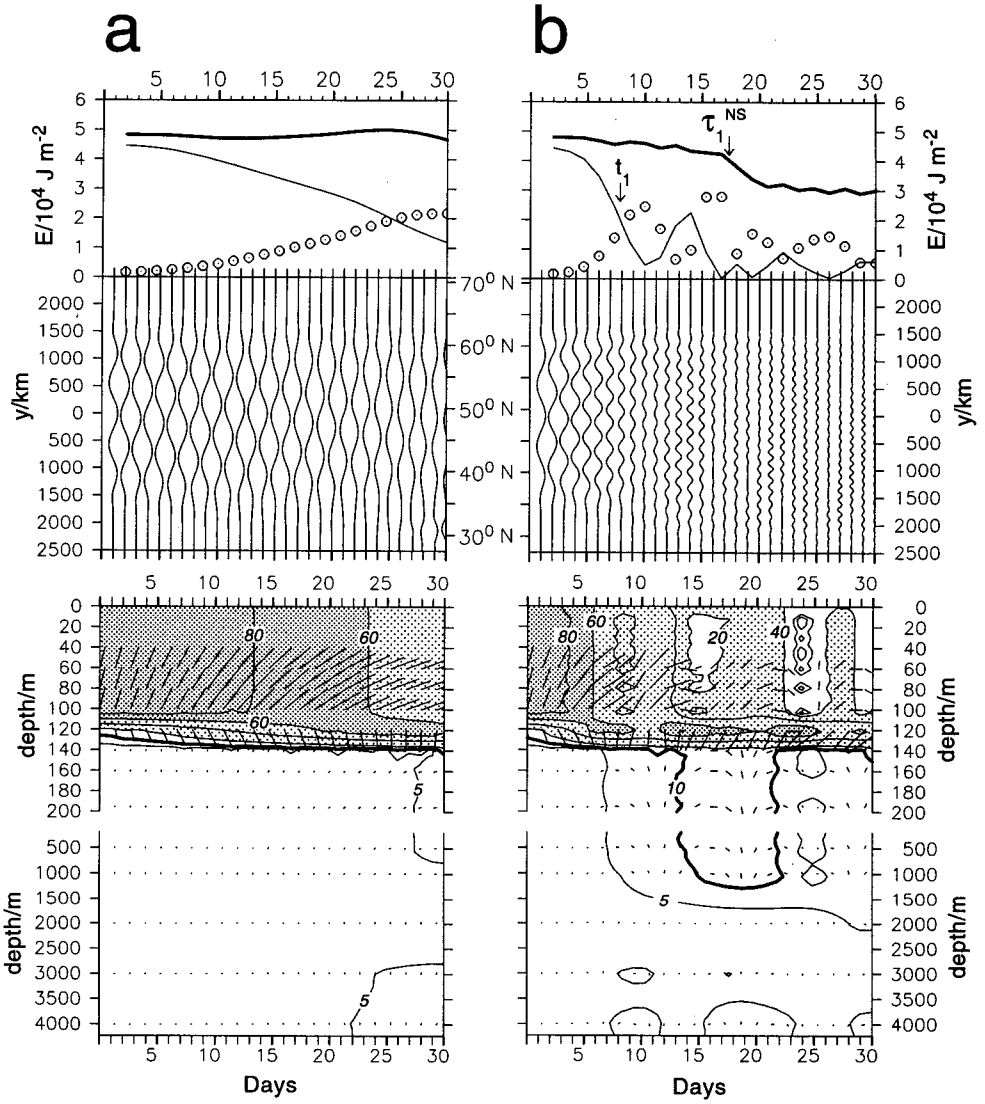

FIG. 7. Example of model results using (a) an f plane and (b) a β plane. Both runs were initialized identically with a small southward propagating meridional wavenumber l_0 = (400 km)$^{-1}$. The top panels display E_T (heavy line), E_{ML} (light line), and E_{PC} (dotted line), at $y = 0$, as a function of time. The middle panels display the u component of mixed layer current as a function of latitude and time. The bottom panel displays inertially backrotated horizontal current vectors sampled at $y = 0$ as a function of depth and time. Superimposed on the stick diagrams are contours of the horizontal current speed in centimeters per second.

30 days causing an additional decrease in E_T. Note that the waves initially going northward (last row, Fig. 8) persist for a longer time before finally propagating away to the south.

The decrease in E_{ML} that is in excess of the decrease in E_T is the result of vertical propagation. Hence, E_{PC} increases as E_{ML} decreases. The timescale t_1 marks when mode 1 first becomes out of phase with f_0 and results in significant vertical propagation. As mentioned in section 4a, subsequent oscillations between E_{ML} and E_{PC} are not easily understood in terms of modal beating. For the case of L_N = 1000 km the effect of inertial beating is clearly evident for mode 1. When L_N = 250 km the timescale t_1 is not relevant as $\tau_1^{NS} < t_1$; hence, mode 1 has left and therefore cannot beat with other modes. However, there is still vertical propagation of energy, but it cannot be explained by beating. In this case the vertical propagation can be understood in terms of the sum of modes. Initially, the sum of modes below the mixed layer was zero. After mode 1 leaves, the sum can no longer be zero. In the mixed layer the amplitude of the inertial oscillation was due to the sum of modes, all in phase. When a mode leaves, the sum has to be smaller. Thus, the departure of the

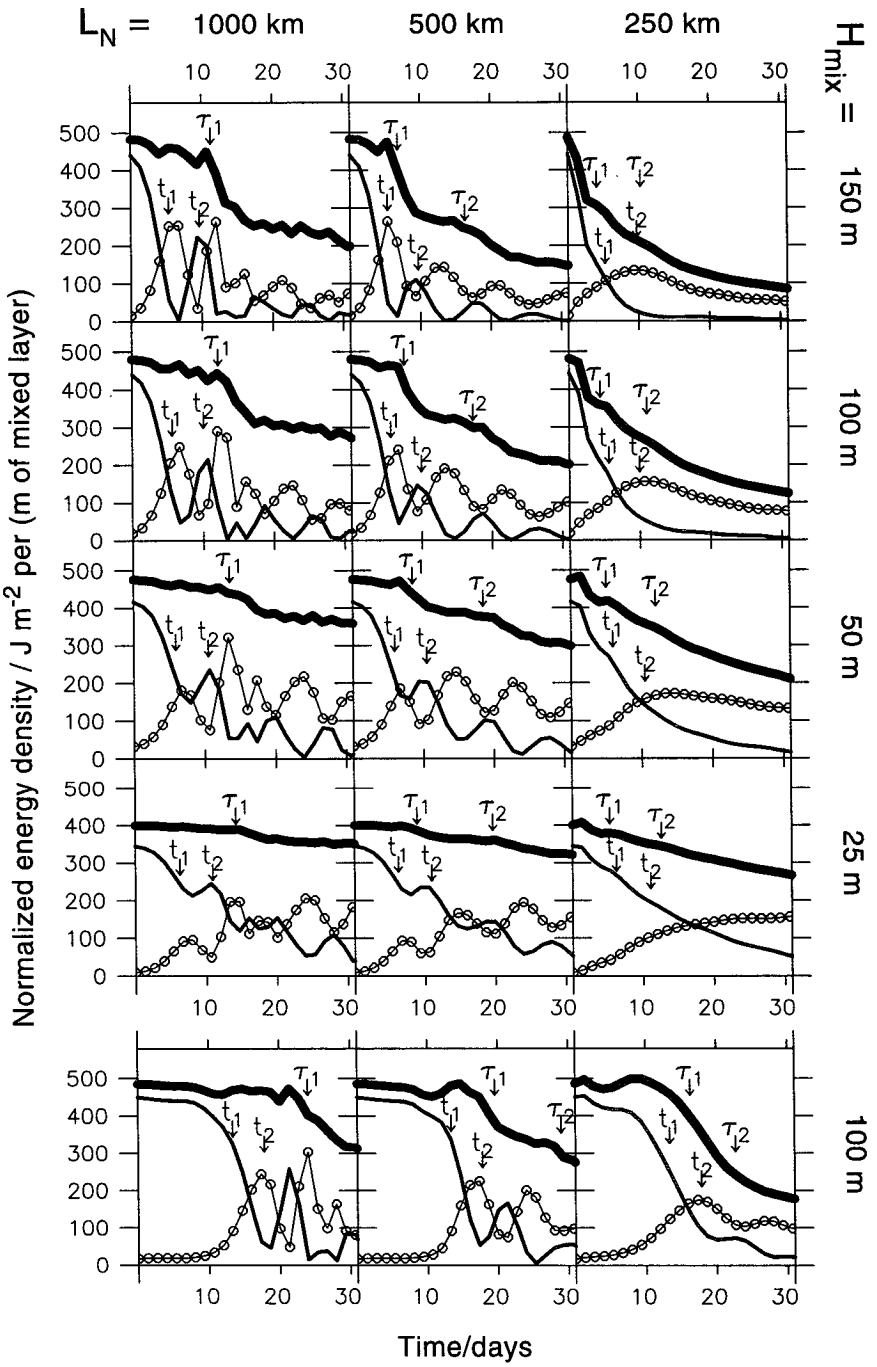

FIG. 8. HKE as a function of time for various model experiments at $y = 0$. Shown are E_T (heavy line), E_{ML} (light line), and E_{PC} (dotted line). The initial wavenumber (k_0, l_0) in the top four rows is $(0, -7.5 \times 10^{-6}\ \text{m}^{-1})$ (southward propagating) and in the bottom row is $(0, +7.5 \times 10^{-6}\ \text{m}^{-1})$ (northward propagating). The value of H_{mix} varies for each row from 150 to 25 m; the northern extent L_N varies for each column from 1000 to 250 km. The timescales t_n and τ_n^{NS} (section 3) are shown for modes 1 and 2. (Note the superscript "NS" has been dropped for clarity.)

low modes results in a downward propagation of energy. For southward propagating initial conditions, the analytically predicted values of t_1 and τ_1^{NS} are in good agreement with the changes of HKE due to vertical and horizontal propagation respectively. Similar timescale arguments for northward propagating initial conditions

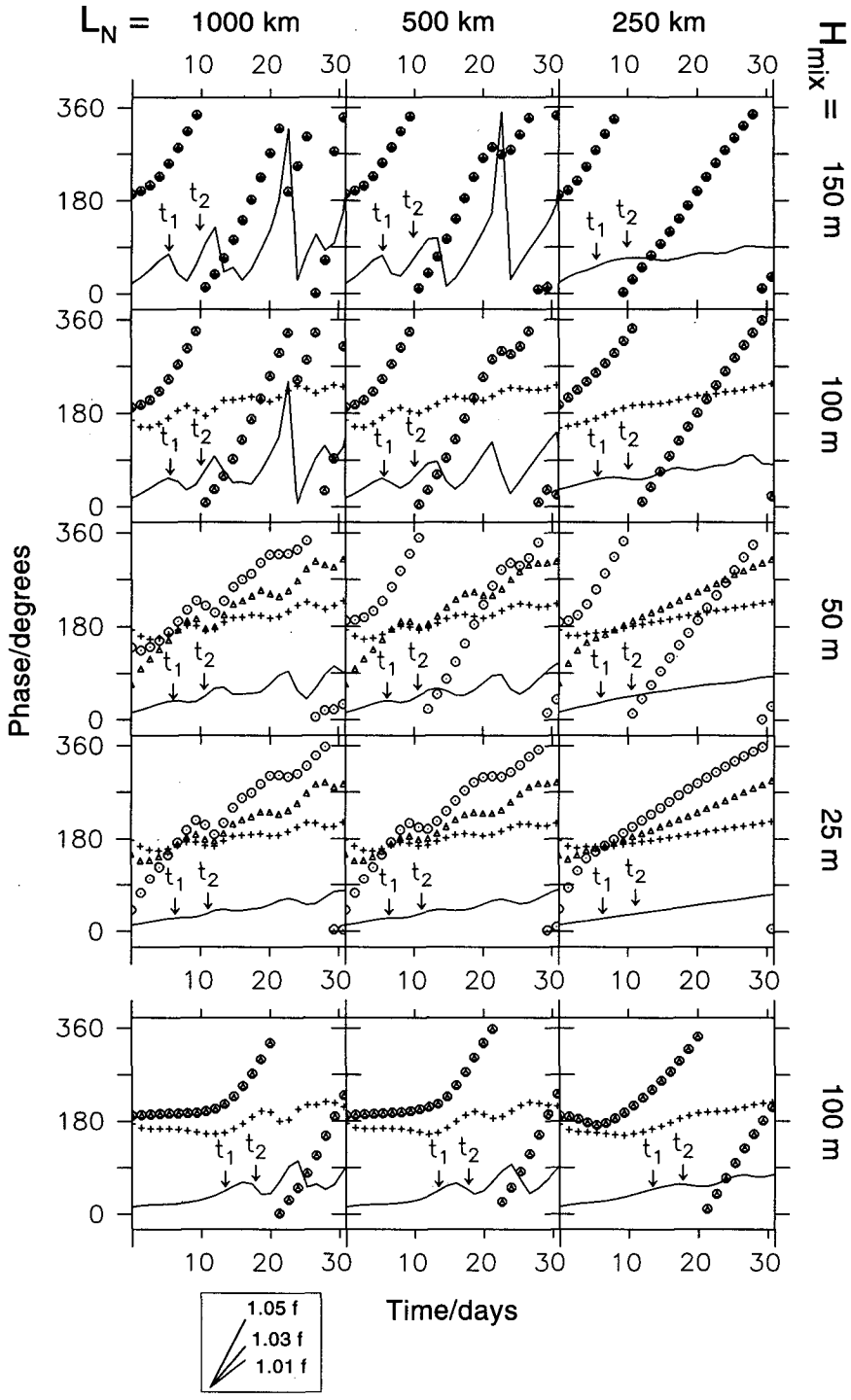

FIG. 9. Backrotated relative phases at selected depths, computed from the same model runs displayed in Fig. 8, shown in the same order. The mixed layer phase is shown with a solid line, and the phase at regular intervals below the mixed layer is shown by different symbols. Displayed are estimates of the current phase in the mixed layer (solid line), and approximately 10 m (+), 20 m (△), and 50 m (⊙) below the base of the mixed layer. A horizontal line denotes a perfectly inertial frequency; a positive slope denotes superinertial frequency. A key for the frequencies is provided on the bottom left corner.

are reasonable (Fig. 8, bottom), but t_1 seems to underestimate the mixed layer decay by a few days.

The detailed phase structure is quite complicated (Fig. 9). The slope of each phase line defines the local frequency at a certain depth; as the currents are back-rotated by f_0, horizontal lines denote perfectly inertial currents. Positive slopes represent superinertial frequencies, while negative slopes correspond to subinertial currents. The distance between phase lines denotes the phase difference with depth, a quantity related to vertical wavenumber; the temporal change of phase difference between two depths reveals the change of vertical structure in time.

The overall frequency changes in time can be understood somewhat by examining the frequency changes of each mode. However, the frequency is the complicated result of adding the contribution from each mode and depends on both the frequency and magnitude of each mode. In general the mixed layer frequency is about $1.005 f_0$, and the frequency increases with depth, resulting in significant phase changes with depth.

c. *Effects of mixed layer depth on the evolution of the wave field*

The quantitative changes in HKE that are associated with the timescales t_n and τ_n^{NS} depend on the relative modal decomposition of the initial condition, that is, upon σ_n. The magnitude of the initial velocity U_0 does not affect the time evolution. The values of σ_n and c_n for the cases shown in Fig. 5 are presented in Table 1 and Fig. 6 for the five lowest modes.

The fraction of energy initially in mode 1, that is, σ_1, increases dramatically with mixed layer depth. This fact can explain much of the model dependence on H_{mix}. As was seen in Fig. 8, at time τ_1^{NS} mode 1 energy leaves $y = 0$ causing a decrease in E_T. The magnitude of the decrease is expected to be related to σ_n. Specifically from Table 1 for $H_{mix} = 25$ m, it is expected that E_T would decrease by 7% by τ_1^{NS}; for $H_{mix} = 150$ m the decrease would be a substantial 42%. These expectations are verified in Fig. 8.

The magnitude of the decrease in E_{ML} due to inertial beating can also be anticipated from the σ_n values. By time t_1 when mode 1 is nearly out of phase with all other modes (destructive interference), it is anticipated that the current speed in the mixed layer would be reduced by $2\sigma_1$, significantly reducing E_{ML}. Hence, this beating effect is expected to be more dramatic for larger H_{mix} as can be seen in Fig. 8. The beating effect is almost absent in the cases of small L_N where $\tau_1^{NS} < t_1$ as mode 1 has left before significant beating occurred.

Note that while changes in the seasonal stratification have a profound effect on σ_n, the effect on c_n is rather small (Fig. 6, Table 1). Mixed layer variation from 25 to 150 m results in changes of c_1 of 20% and less than 5% for higher modes. This is a significant result because it means that the timescale of the wave evolution is not a strong function of mixed layer depth, while the magnitude of the decrease is.

d. *Effects of deep stratification on the wave evolution*

In addition to the mixed layer depth (seasonal stratification) the variations in the deep stratification affect wave propagation. Since we have found that some of the features of the numerical model results can be explained by analytical wave propagation, we will assess the role of deep stratification without explicitly solving the numerical model.

Vertical profiles of zonally averaged temperature and salinity for the Atlantic and Pacific Oceans were obtained from Levitus (1982). Assuming a 50-m mixed layer in all cases, $N(z)$ was calculated and values of c_n and σ_n were estimated by modal decomposition for various latitude bands (Tables 2 and 3, Fig. 10).

In most of these profiles σ_n has a maximum at a mode greater than 1. At 47.5°N in the Atlantic Ocean, modes 4 and 5 are more energetic than modes 1, 2, and 3 combined. This behavior of σ_n is not found in the idealized $N(z)$ profile (35). For waves propagating in these average stratifications, the model will behave as discussed above, but mode 1 will have proportionately less impact on the solution than with the idealized $N(z)$, since the relative importance of each mode is given by σ_n.

The values of c_n also vary with stratification. The weaker deep stratification toward the poles leads to

TABLE 1. Values of eigenspeed c_n and modal coefficient σ_n for the first five modes, calculated for the idealized stratification profiles shown in Fig. 6.

	$H_{mix} = 25$ m		$H_{mix} = 50$ m		$H_{mix} = 100$ m		$H_{mix} = 150$ m	
Mode	c_n (m s^{-1})	σ_n	c_n (m s^{-1})	σ_n	c_n (m s^{-1})	σ_n	c_n (m s^{-1})	σ_n
1	2.35	0.07	2.45	0.15	2.63	0.30	2.82	0.42
2	1.28	0.08	1.34	0.15	1.42	0.21	1.47	0.21
3	0.87	0.08	0.90	0.12	0.94	0.12	0.95	0.10
4	0.66	0.07	0.67	0.09	0.69	0.07	0.70	0.06
5	0.53	0.06	0.54	0.07	0.54	0.05	0.55	0.03

TABLE 2. Values of eigenspeed c_n and modal coefficient σ_n for the first five modes, calculated for zonally averaged stratification profiles from the Atlantic Ocean.

	47.5°N		27.5°N		32.5°S		67.5°S	
Mode	c_n (m s^{-1})	σ_n	c_n (m s^{-1})	σ_n	c_n (m s^{-1})	σ_n	c_n (m s^{-1})	σ_n
1	2.79	0.07	3.78	0.09	3.61	0.07	1.02	0.05
2	1.40	0.05	1.65	0.11	1.76	0.08	0.53	0.26
3	0.92	0.08	1.20	0.17	1.19	0.07	0.30	0.14
4	0.68	0.12	0.94	0.12	0.93	0.13	0.24	0.04
5	0.56	0.13	0.74	0.06	0.75	0.11	0.20	0.06

lower values of c_n. However, the dependence of c_n on mode remains nearly proportional to n^{-1}.

Both frequency and group velocity of the waves are functions of $c_n^2 f_0^{-1}$. At high latitudes, weaker stratification and high f_0 cause the vertical and horizontal propagation of energy to be much slower than the idealized midlatitude case examined above. This is seen in estimates of t_1 and τ_1^{NS} (Fig. 11a). In contrast, at lower latitudes stronger stratification and smaller f_0 result in faster wave propagation and shorter timescales (Fig. 11b). Hence, it appears that variations in both deep stratification and latitude can be equally responsible in determining the evolution timescales of the wave field.

e. *Conditions for a two-dimensional approximation*

It has been a common practice in past modeling efforts to consider only two-dimensions: depth and one horizontal dimension. The reasons for using a two-dimensional model are obvious: both the analytical and the numerical relations are simpler and the numerical schemes are easier to run. Price (1983) and Kundu and Thomson (1985) used f planes and aligned the x axis with the direction of propagation of the atmospheric front. This simplification is always possible and exact in an f plane.

In a β plane the two-dimensional assumption is made by neglecting k, the zonal component of the wavenumber (e.g., G84; D'Asaro 1989). This is often reasonable since k_0 is often small and k is constant in time. In contrast, l increases as βt; so no matter how small l_0 is, l will eventually be large enough to generate significant vertical propagation.

To determine the conditions for which k can be neglected, we first consider the effect of k on the frequency given by the dispersion relation (21). We compare the frequency ω_{n0} for $k = 0$, with the frequency ω_{nk} for $k = k_0$. These two frequencies will be considered to be sufficiently close for times less than $\bar{t}_n$, where $\bar{t}_n$ is defined when the phase difference between the two frequencies reaches $\pi/4$, that is, where $(\omega_{n0} - \omega_{nk})\bar{t}_n = \pi/4$. Since we are in the parameter range where k is small, we assume ϵ is small and use (30) to estimate $\bar{t}_n$ explicitly as

$$\bar{t}_n = \frac{\pi}{2} \frac{f_0}{c_n^2 k_0^2}. \tag{37}$$

Note that $\bar{t}_n$ is independent of l_0 and depends only on k_0, stratification, and f_0. If we consider the full dispersion relation (21) ($\epsilon \neq 0$), $\bar{t}_n$ varies slowly with l_0. Since mode 1 always has the highest frequency, for a given k_0, the zonal dependence can be neglected in the model for times less than $\bar{t}_1$. Figure 12 shows $\bar{t}_1$ as a function of k_0 for the idealized $N(z)$ profile at midlatitudes (50°N), as well as the extreme cases of zonal averages of $N(z)$ at low latitudes (27.5°N) and high latitudes (67.5°S). For the midlatitude case, at $k_0 = 10^{-5}$ m^{-1} (a scale of 100 km), $\bar{t}_1 = 3$ days, and k dependence can be neglected only for times less than 3 days. However, at a larger scale of $k_0 = 2 \times 10^{-6}$ m^{-1} (scale of 500 km), $\bar{t}_1 = 70$ days.

5. Summary and conclusions

A time-varying wind stress generates current oscillations in the upper ocean. Significant generation often

TABLE 3. Values of eigenspeed c_n and modal coefficient σ_n for the first five modes, calculated for zonally averaged stratification profiles from the Pacific Ocean.

	47.5°N		27.5°N		32.5°S		57.5°S	
Mode	c_n (m s^{-1})	σ_n	c_n (m s^{-1})	σ_n	c_n (m s^{-1})	σ_n	c_n (m s^{-1})	σ_n
1	2.94	0.09	4.11	0.11	3.66	0.08	2.56	0.06
2	1.52	0.14	1.98	0.11	1.80	0.14	1.26	0.04
3	1.05	0.14	1.34	0.12	1.26	0.06	0.84	0.06
4	0.80	0.08	1.01	0.09	0.93	0.06	0.64	0.06
5	0.63	0.04	0.81	0.07	0.75	0.09	0.51	0.08

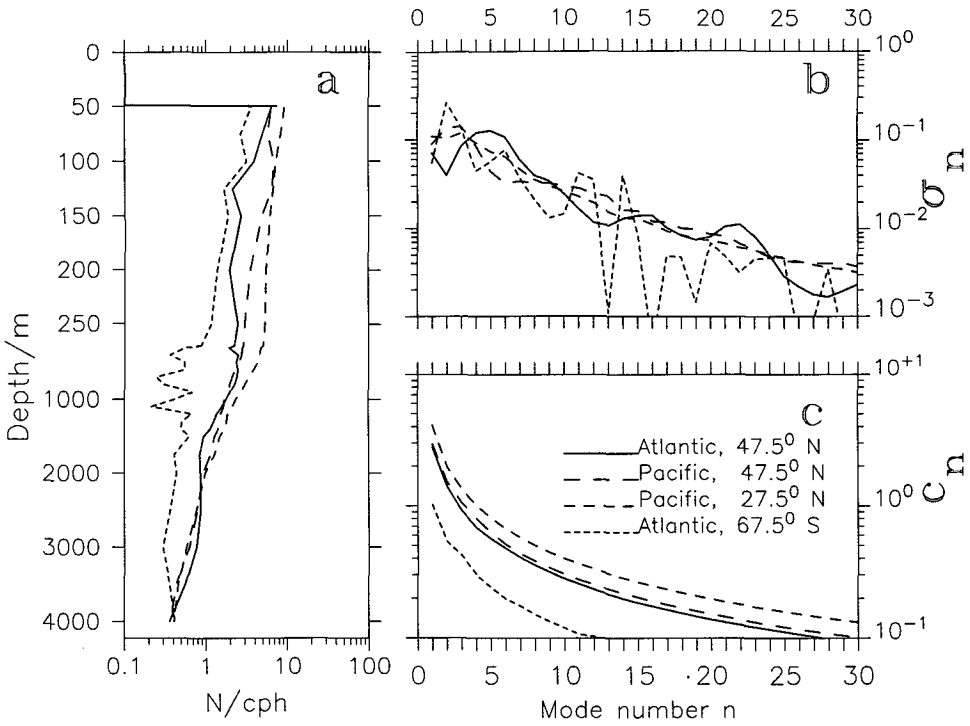

FIG. 10. As in Fig. 6 but for historical hydrographic profiles with an imposed 50-m mixed layer. Note that there are significant variations in the relative weights of the low modes. Significant variations in eigenspeed are correlated with the overall strength of the deep stratification: high stratification results in high eigenspeeds.

occurs with the passing of a storm front that locally lasts for hours; generation can persist over a large area before the front weakens. After the storm event, the oscillations created in the upper ocean can radiate vertically and horizontally as near-inertial gravity waves.

The goal of this paper is to characterize the radiation of near-inertial waves from the mixed layer that is consistent with linear, inviscid dynamics on a β plane (section 2). We find, by comparing a numerical model with analytical theory, that predictions of some features of the wave evolution can be made without the need to run the numerical model. Specifically we investigate the timescales and magnitude of energy propagation as a function of initial conditions and background properties.

The numerical model is patterned after the initial-value problem introduced by G84, where vertical modes are used to represent the vertical structure. The numerical model differs from the one developed in G84 by

- adding the third spatial dimension, thereby permitting zonal gradients,
- limiting the horizontal extent of the storm to an arbitrary scale, and
- setting the initial condition in the mixed layer to be consistent with the passing of a fast moving front.

The propagation of modes at distinct frequencies and horizontal group speeds results in vertical propagation of energy that can be explained by two mechanisms: modal interference and modal departure.

When the horizontal extent of the initial mixed layer currents is large, the vertical propagation of energy may be explained by the interference of modes oscillating at different frequencies—a phenomenon known as inertial beating (G84). The timescale t_n is defined as the time mode n becomes out of phase (beats) with higher modes, which oscillate at a frequency closer to f. The beating of mode 1 at t_1 marks the first time effective vertical propagation of energy occurs. The value of t_1 depends greatly on the initial wavenumber of the currents in the mixed layer. The β effect causes a significant difference in t_1 between an initially northward or southward propagating front; inertial beating occurs sooner for a southward going front (Fig. 3a). The depth of the mixed layer is not a significant variable in determining t_n (Fig. 6) as c_n varies little with mixed layer depth.

For initial conditions of finite horizontal extent, vertical propagation of energy may also be explained by the successive departure of modes from the generation area. To describe this process, we have defined the timescales τ_n^{NS} and τ_n^{EW}, representing the times when mode n leaves $y = 0$ due to north–south and east–west extent respectively. These timescales are a function of the horizontal extent of the storm as well as the initial wavenumber (Fig. 3b). For example, when mode 1

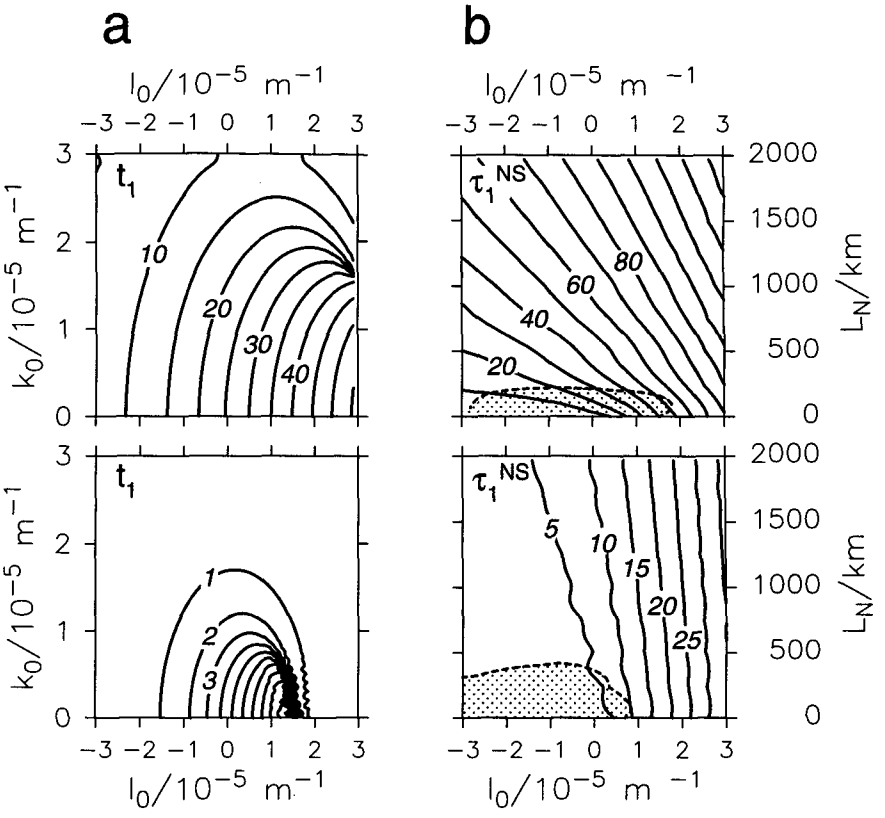

FIG. 11. Contours of timescales t_1 and τ_1^{NS} in days, calculated for the extreme stratification profiles in Fig. 10 at 67.5°S (top panels) and at 27.5°N (bottom panels). The format is the same as in Fig. 3.

leaves, the total energy is reduced, but the reduction is not uniform throughout the water column.

Beside the initial wavenumber all the timescales are affected by the modal eigenspeeds c_n and the value of f_0. Hence, variations in deep stratification and latitude will affect the timescales. Some examples from climatological averages show that the timescales that characterize the evolution of the near-inertial wave field vary from a few days at low latitudes to several weeks at high (Fig. 11).

While the quantities t_n, τ_n^{NS}, and τ_n^{EW} determine the timescales of vertical propagation, the quantitative effect of the inertial beating and modal departure is determined by the modal composition of the wave field σ_n. For example, if mode 1 is a large fraction of the total energy (σ_1 large), then the vertical propagation that occurs by t_1 will be significant. The modal composition varies with stratification—the deeper the mixed layer the larger the mode 1 contribution. Hence, the energy transfers at times t_1 and τ_1^{NS} are more dramatic for deeper mixed layers (Fig. 8). This modal description is most useful when the low modes dominate. As the partition of energy among modes becomes more uniform, the energy transfers that occur at t_n and τ_n^{NS} will smear into a continuum.

From the two processes described by the model, it is modal interference that may be associated with observed energy oscillations between the mixed layer and pycnocline. When modal departure is the dominant mechanism of downward propagation of energy, energy leaving the mixed layer does not return.

This analysis also permits us to develop criteria for which the model can be simplified. The zonal dependence can be neglected for sufficiently small k_0, thereby reducing the problem to two dimensions (Fig. 12).

The linear, numerical model developed here provides us with the confidence to use analytical theory to describe some aspects of the evolution of the inertial wave field generated by a large, fast storm propagating at any direction. However, to assess the usefulness of this model, comparisons with oceanic observations are needed. One such comparison is made using observations from Ocean Storms in Levine and Zervakis (1995).

Acknowledgments. We thank Eric D'Asaro for his persistent leadership throughout Ocean Storms. Discussions with Clayton Paulson and Roland de Szoeke were greatly appreciated. The comments of the anon-

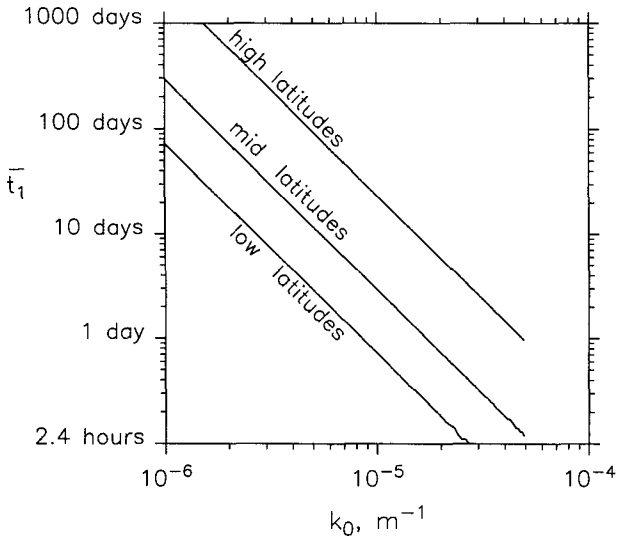

FIG. 12. Timescale $\bar{t}_1$ as a function of initial meridional wavenumber k_0. For times less than $\bar{t}_1$ the zonal dimension in the model can be neglected.

ymous reviewers were useful in improving the manuscript. Thanks to the Office of Naval Research for their support through Contracts N00014-84-C-0218 and N00014-87-K-0009, and Grant N00014-90-J-1048.

REFERENCES

Anderson, D. L., and A. E. Gill, 1979: Beta dispersion of inertial waves. *J. Geophys. Res.*, **84,** 1836–1842.

D'Asaro, E., 1985: The energy flux from the wind to near-inertial motions in the surface mixed layer. *J. Phys. Oceanogr.*, **15,** 1043–1059.

——, 1989: The decay of wind-forced mixed layer inertial oscillations due to the beta effect. *J. Geophys. Res.*, **94,** 2045–2056.

——, C. C. Erikson, M. D. Levine, P. P. Niiler, C. A. Paulson, and P. Van Meurs, 1995: Upper ocean inertial currents forced by a strong storm. Part I: Data and comparisons with linear theory. *J. Phys. Oceanogr.*, **25,** 2909–2936.

Gill, A. E., 1982: *Atmosphere–Ocean Dynamics.* Academic Press, 346–353.

——, 1984: On the behavior of internal waves in the wakes of storms. *J. Phys. Oceanogr.*, **14,** 1129–1151.

Greatbatch, R. J., 1983: On the response of the ocean to a moving storm: The non-linear dynamics. *J. Phys. Oceanogr.*, **13,** 357–367.

——, 1984: On the response of the ocean to a moving storm: Parameters and Scales. *J. Phys. Oceanogr.*, **14,** 59–78.

Higdon, R. L., 1994: Radiation boundary conditions for dispersive waves. *SIAM J. Num. Anal.*, **31,** 64–100.

Kundu, P. K., 1976: An analysis of inertial oscillations observed near Oregon coast. *J. Phys. Oceanogr.*, **6,** 879–893.

——, 1986: A two-dimensional model of inertial oscillations generated by a propagating wind-field. *J. Phys. Oceanogr.*, **16,** 1399–1411.

——, 1993: On internal waves generated by traveling wind. *J. Fluid Mech.*, **254,** 529–559.

——, and R. E. Thomson, 1985: Inertial oscillations due to a moving front. *J. Phys. Oceanogr.*, **15,** 1076–1084.

Levitus, S., 1982: *Climatological Atlas of the World Ocean.* Prof. Paper No. 13, National Oceanic and Atmospheric Administration, U.S. Department of Commerce, Rockville, MD.

Levine, M. D., and V. Zervakis, 1995: Near-inertial wave propagation into the pycnocline during ocean storms: Observations and model comparison. *J. Phys. Oceanogr.*, **25,** 2890–2908.

Lighthill, J., 1978: *Waves in Fluids.* Cambridge University Press, 317–325.

Paduan, J., R. A. deSzoeke, and R. A. Weller, 1989: Inertial oscillations in the upper ocean during the mixed layer dynamics of the Upper Ocean Experiment. *J. Geophys. Res.*, **94**(C4), 4835–4842.

Pollard, R. T., 1970: On the generation by winds of inertial waves in the ocean. *Deep-Sea Res.*, **17,** 795–812.

——, and R. C. Millard, 1970: Comparison between observed and simulated wind-generated inertial oscillations. *Deep-Sea Res.*, **17,** 813–821.

Price, J. G., 1983: Internal wave wake of a moving storm. Part I: Scales, energy budget, and observations. *J. Phys. Oceanogr.*, **13,** 949–965.

Rubenstein, D. M., 1983: Vertical dispersion of inertial waves in the upper ocean. *J. Geophys. Res.*, **88,** 4368–4380.

Shay, L. K., and R. L. Elsberry, 1987: Near-inertial ocean current response to hurricane Frederick. *J. Phys. Oceanogr.*, **17,** 1249–1269.